R-FUSE: Robust Fast Fusion of Multiband Images Based on Solving a Sylvester Equation

Qi Wei, *Member, IEEE*, Nicolas Dobigeon, *Senior Member, IEEE*, Jean-Yves Tourneret, *Senior Member, IEEE*, José Bioucas-Dias, *Senior Member, IEEE*, and Simon Godsill, *Member, IEEE*

***Abstract*—This letter proposes a robust fast multiband image fusion method to merge a high-spatial low-spectral resolution image and a low-spatial high-spectral resolution image. Following the method recently developed by Wei *et al.*, the generalized Sylvester matrix equation associated with the multiband image fusion problem is solved in a more robust and efficient way by exploiting the Woodbury formula, avoiding any permutation operation in the frequency domain as well as the blurring kernel invertibility assumption required in their method. Thanks to this improvement, the proposed algorithm requires fewer computational operations and is also more robust with respect to the blurring kernel compared with the one developed by Wei *et al.* The proposed new algorithm is tested with different priors considered by Wei *et al.* Our conclusion is that the proposed fusion algorithm is more robust than the one by Wei *et al.* with a reduced computational cost.**

***Index Terms*—Circulant matrix, multiband image fusion, Sylvester equation, Woodbury formula.**

I. Introduction

A. Background

THE multiband image fusion problem, i.e., fusing hyperspectral (HS) and multispectral (MS)/panchromatic (PAN) images, has recently been receiving particular attention in remote sensing [2]. High spectral resolution multiband imaging generally suffers from the limited spatial resolution of the data acquisition devices, mainly due to an unavoidable tradeoff between spatial and spectral sensitivities [3]. For example, HS images benefit from excellent spectroscopic properties with hundreds of bands but are limited by their relatively low spatial resolution compared to MS and PAN images (that are acquired in much fewer bands). As a consequence, reconstructing a high-spatial and high-spectral multiband image from two degraded and complementary observed images is a challenging but crucial issue that has been addressed in various scenarios [4]–[7]. In particular, fusing a high-spatial low-spectral resolution image and a low-spatial high-spectral image is an archetypal instance of multiband image reconstruction, such as pansharpening [8] or HS pansharpening [2]. Generally, the linear degradations applied to the observed images with respect to (w.r.t.) the target high-spatial and high-spectral image reduce to spatial and spectral transformations. Thus, the multiband image fusion problem can be interpreted as restoring a three-dimensional data-cube from two degraded data-cubes. A detailed formulation is presented below.

Manuscript received April 6, 2016; revised June 6, 2016, July 14, 2016, and August 19, 2016; accepted September 6, 2016. Date of publication September 13, 2016; date of current version October 3, 2016. This work was supported in part by the ERA-NET MED MapInvPlnt Project no. ANR-15-NMED-0002-02 and ERANETMED/0001/2014, in part by the Hypanema ANR Project no. ANR-12-BS03-003 and FCT-ERANETMED/0001/2014, and in part by ANR-11-LABX-0040-CIMI within the program ANR-11-IDEX-0002-02 within the thematic trimester on image processing, and in part by the Portuguese Fundacãopara a Ciência e Tecnologia (FCT) under grant UID/EEA/5008/2013. The associate editor coordinating the review of this manuscript and approving it for publication was Dr. Sanghoon Lee.

Q. Wei and S. Godsill are with the Department of Engineering, University of Cambridge, Cambridge CB2 1PZ, U.K. (e-mail: qi.wei@eng.cam.ac.uk; sjg@eng.cam.ac.uk).

N. Dobigeon and J.-Y. Tourneret are with the University of Toulouse, IRIT/INP-ENSEEIHT, 2 rue Camichel, BP 7122, 31071 Toulouse cedex 7, France (e-mail: nicolas.dobigeon@enseeiht.fr; jean-yves.tourneret@enseeiht.fr).

J. Bioucas-Dias is with the Instituto de Telecomunicações and Instituto Superior Técnico, Universidade de Lisboa, Lisboa 1049-001, Portugal (e-mail: {bioucas}@lx.it.pt).

Color versions of one or more of the figures in this letter are available online at http://ieeexplore.ieee.org.

Digital Object Identifier 10.1109/LSP.2016.2608858

B. Problem Statement

This work directly follows the formulation of [1] and uses the well-admitted linear degradation model

$$\begin{aligned}\mathbf{Y}_{\mathrm{L}} &= \mathbf{L}\mathbf{X} + \mathbf{N}_{\mathrm{L}} \\ \mathbf{Y}_{\mathrm{R}} &= \mathbf{X}\mathbf{B}\mathbf{S} + \mathbf{N}_{\mathrm{R}}\end{aligned} \tag{1}$$

where

- $\mathbf{X} \in \mathbb{R}^{m_\lambda \times n}$ is full resolution target image;
- $\mathbf{Y}_{\mathrm{L}} \in \mathbb{R}^{n_\lambda \times n}$ and $\mathbf{Y}_{\mathrm{R}} \in \mathbb{R}^{m_\lambda \times m}$ are observed spectrally degraded and spatially degraded images;
- $\mathbf{L} \in \mathbb{R}^{n_\lambda \times m_\lambda}$ is spectral response of the sensor;
- $\mathbf{B} \in \mathbb{R}^{n \times n}$ is cyclic convolution operator on the bands;
- $\mathbf{S} \in \mathbb{R}^{n \times m}$ is d uniform downsampling operator, which has $m = n/d$ ones on the block diagonal and zeros elsewhere, such that $\mathbf{S}^H\mathbf{S} = \mathbf{I}_m$;
- $\mathbf{N}_{\mathrm{L}} \in \mathbb{R}^{n_\lambda \times n}$ and $\mathbf{N}_{\mathrm{R}} \in \mathbb{R}^{m_\lambda \times m}$ are additive noise terms assumed to be distributed according to matrix normal distributions [9]

$$\begin{aligned}\mathbf{N}_{\mathrm{L}} &\sim \mathcal{MN}_{n_\lambda, n}(\mathbf{0}_{n_\lambda, n}, \mathbf{\Lambda}_{\mathrm{L}}, \mathbf{I}_n) \\ \mathbf{N}_{\mathrm{R}} &\sim \mathcal{MN}_{m_\lambda, m}(\mathbf{0}_{m_\lambda, m}, \mathbf{\Lambda}_{\mathrm{R}}, \mathbf{I}_m)\end{aligned}$$

where $\mathbf{\Lambda}_{\mathrm{L}}$ and $\mathbf{\Lambda}_{\mathrm{R}}$ denotes the noise covariance matrices depending on the sensors. Note that n_λ and m_λ are the numbers of bands in $\mathbf{Y}_{\mathrm{L}}$ and $\mathbf{Y}_{\mathrm{R}}$, respectively, and that n and m are the numbers of pixels per band in $\mathbf{Y}_{\mathrm{L}}$ and $\mathbf{Y}_{\mathrm{R}}$.

Computing the maximum likelihood (ML) or the Bayesian estimates (associated with any prior) of $\mathbf{X}$ from $\mathbf{Y}_{\mathrm{L}}$ and $\mathbf{Y}_{\mathrm{R}}$ is a challenging task, mainly due to the large size of $\mathbf{X}$ and due to the presence of the downsampling operator $\mathbf{S}$, which prevents any direct use of the Fourier transform (FT) to diagonalize the joint spatial degradation operator $\mathbf{BS}$. To overcome this difficulty, several computational strategies have been designed to

approximate the estimators. One strategy is using a Markov chain Monte Carlo (MCMC) method to generate samples asymptotically distributed according to the posterior distribution of $\mathbf{X}$ [10]. Despite this formal appeal, MCMC-based methods have the major drawback of being computationally expensive, which prevents their effective use when processing images of large size. Another strategy developed in [11] exploited a block coordinate descent (BCD) method to compute the maximum *a posteriori* (MAP) estimator of $\mathbf{X}$, greatly decreasing the complexity compared to its MCMC counterpart. Based on a prior built from a sparse representation, the fusion problem was solved in [12] and [13] with the split augmented Lagrangian shrinkage algorithm (SALSA) [14]. In [1], contrary to the algorithms described above, a much more efficient method was proposed to solve explicitly an underlying Sylvester equation (SE) derived from (1), leading to an algorithm referred to as Fast fUsion based on Sylvester Equation (FUSE). This algorithm can be implemented *per se* to compute the ML estimate of $\mathbf{X}$ efficiently and has also the great advantage of being easily generalizable within a Bayesian framework when considering various priors (see the corresponding technical report [15] with more experimental results). The MAP estimates of $\mathbf{X}$ associated with a Gaussian prior similar to the one considered in [10] and [11] can be directly computed thanks to the proposed strategy. When handling more complex priors such as those used in [12] and [13], the FUSE solution can be conveniently embedded within a conventional alternating direction method of multipliers (ADMM) or a BCD algorithm. Note that the FUSE algorithm requires the nontrivial assumption that the blurring matrix $\mathbf{B}$ is invertible, which is not always guaranteed in practice.

Inspired by recent works on single image super-resolution [16], [17], we propose a more robust version of the FUSE algorithm, which is referred to as R-FUSE. The R-FUSE algorithm computes the FT of the target image explicitly using the Woodbury formula. A direct consequence of this modification is to get rid of the invertibility assumption for the blurring matrix $\mathbf{B}$. A side product of this modification is that the permutations conducted in the frequency domain (characterized by matrix $\mathbf{P}$ in [1]) are no longer required in the R-FUSE algorithm.

II. Problem Formulation

Since adjacent HS bands are known to be highly correlated, the columns of $\mathbf{X}$ usually lie in a subspace whose dimension $\widetilde{m}_\lambda$ is much smaller than the number of bands m_λ [18], [19], i.e., $\mathbf{X} = \mathbf{HU}$ where $\mathbf{H}$ is a full column rank matrix and $\mathbf{U} \in \mathbb{R}^{\widetilde{m}_\lambda \times n}$ is the coefficients of $\mathbf{X}$ onto the subspace spanned by the columns of $\mathbf{H} \in \mathbb{R}^{m_\lambda \times \widetilde{m}_\lambda}$. According to the ML or least-squares principles, the fusion problem associated with the linear model (1) can be formulated as

$$\min_{\mathbf{U}} L(\mathbf{U}) \tag{2}$$

where

$$L(\mathbf{U}) = \|\mathbf{\Lambda}_{\mathrm{R}}^{-\frac{1}{2}} \left(\mathbf{Y}_{\mathrm{R}} - \mathbf{HUBS}\right)\|_F^2 + \|\mathbf{\Lambda}_{\mathrm{L}}^{-\frac{1}{2}} \left(\mathbf{Y}_{\mathrm{L}} - \mathbf{LHU}\right)\|_F^2$$

and $\|\cdot\|_F$ represents the Frobenius norm.

III. Robust Fast Fusion Scheme

A. Sylvester Equation

Minimizing (2) w.r.t. $\mathbf{U}$ is equivalent to force the derivative of $L(\mathbf{U})$ to be zero, i.e., $\nabla L(\mathbf{U}) = 0$, leading to the following matrix equation

$$\begin{aligned}&\mathbf{H}^H \mathbf{\Lambda}_{\mathrm{R}}^{-1} \mathbf{HUBS} \left(\mathbf{BS}\right)^H + \left(\left(\mathbf{LH}\right)^H \mathbf{\Lambda}_{\mathrm{L}}^{-1} \mathbf{LH}\right) \mathbf{U} \\ &= \mathbf{H}^H \mathbf{\Lambda}_{\mathrm{R}}^{-1} \mathbf{Y}_{\mathrm{R}} \left(\mathbf{BS}\right)^H + \left(\mathbf{LH}\right)^H \mathbf{\Lambda}_{\mathrm{L}}^{-1} \mathbf{Y}_{\mathrm{L}}.\end{aligned} \tag{3}$$

As mentioned in Section I-B, the difficulty for solving (3) results from the high dimensionality of $\mathbf{U}$ and the presence of the downsampling matrix $\mathbf{S}$. The work in [1] showed that (3) can be solved analytically with the following two assumptions:

1) The blurring matrix $\mathbf{B}$ is a block circulant matrix with circulant blocks.
2) The decimation matrix $\mathbf{S}$ corresponds to downsampling the original image and its conjugate transpose $\mathbf{S}^H$ interpolates the decimated image with zeros.

As a consequence, the matrix $\mathbf{B}$ can be decomposed as $\mathbf{B} = \mathbf{FDF}^H$ with $\mathbf{B}^H = \mathbf{FD}^*\mathbf{F}^H$, where $\mathbf{F} \in \mathbb{R}^{n \times n}$ is the discrete FT (DFT) matrix ($\mathbf{FF}^H = \mathbf{F}^H\mathbf{F} = \mathbf{I}_n$), $\mathbf{D} \in \mathbb{R}^{n \times n}$ is a diagonal matrix, and $*$ represents the conjugate operator. Another nontrivial assumption used in [1] is that the matrix $\mathbf{D}$ (or equivalently $\mathbf{B}$) is invertible, which is not necessary in this work as shown in Section III-B. In practice, the matrix $\mathbf{D}$ is often noninvertible as the deconvolution is an ill-posed problem [20], [21]. The decimation matrix satisfies the property $\mathbf{S}^H\mathbf{S} = \mathbf{I}_m$ and the matrix $\underline{\mathbf{S}} \triangleq \mathbf{SS}^H$ is symmetric and idempotent, i.e., $\underline{\mathbf{S}} = \underline{\mathbf{S}}^H$ and $\underline{\mathbf{S}}\underline{\mathbf{S}}^H = \underline{\mathbf{S}}$. For a practical implementation, multiplying an image by $\underline{\mathbf{S}}$ can be achieved by doing entry-wise multiplication with an $n \times n$ mask matrix with ones at the sampled position and zeros elsewhere.

After multiplying (3) on both sides by $\left(\mathbf{H}^H \mathbf{\Lambda}_{\mathrm{R}}^{-1} \mathbf{H}\right)^{-1}$, we obtain

$$\mathbf{C}_1\mathbf{U} + \mathbf{UC}_2 = \mathbf{C} \tag{4}$$

where

$$\begin{aligned}\mathbf{C}_1 &= \left(\mathbf{H}^H \mathbf{\Lambda}_{\mathrm{R}}^{-1} \mathbf{H}\right)^{-1} \left(\left(\mathbf{LH}\right)^H \mathbf{\Lambda}_{\mathrm{L}}^{-1} \mathbf{LH}\right) \\ \mathbf{C}_2 &= \mathbf{B}\underline{\mathbf{S}}\mathbf{B}^H \\ \mathbf{C} &= \left(\mathbf{H}^H \mathbf{\Lambda}_{\mathrm{R}}^{-1} \mathbf{H}\right)^{-1} \left(\mathbf{H}^H \mathbf{\Lambda}_{\mathrm{R}}^{-1} \mathbf{Y}_{\mathrm{R}} \left(\mathbf{BS}\right)^H + \left(\mathbf{LH}\right)^H \mathbf{\Lambda}_{\mathrm{L}}^{-1} \mathbf{Y}_{\mathrm{L}}\right).\end{aligned} \tag{5}$$

Equation (4) is a Sylvester matrix equation that admits a unique solution if and only if an arbitrary sum of the eigenvalues of $\mathbf{C}_1$ and $\mathbf{C}_2$ is not equal to zero [22].

B. Proposed Closed-Form Solution

Using the eigendecomposition $\mathbf{C}_1 = \mathbf{Q\Lambda Q}^{-1}$ and multiplying both sides of (4) by $\mathbf{Q}^{-1}$ leads to

$$\mathbf{\Lambda Q}^{-1}\mathbf{U} + \mathbf{Q}^{-1}\mathbf{UC}_2 = \mathbf{Q}^{-1}\mathbf{C}. \tag{6}$$

Right multiplying (6) by the DFT matrix $\mathbf{F}$ on both sides and using the definitions of matrices $\mathbf{C}_2$ and $\mathbf{B}$ yields

$$\mathbf{\Lambda Q}^{-1}\mathbf{UF} + \mathbf{Q}^{-1}\mathbf{UF}\left(\mathbf{DF}^H\underline{\mathbf{S}}\mathbf{FD}^*\right) = \mathbf{Q}^{-1}\mathbf{CF}. \tag{7}$$

Note that $\mathbf{UF} \in \mathbb{R}^{\widetilde{m}_\lambda \times n}$ is the FT of the target image, which is a complex matrix. Equation (7) can be regarded as an SE w.r.t. $\mathbf{Q}^{-1}\mathbf{UF}$, which has a simpler form compared to (4) as $\mathbf{\Lambda}$ is a diagonal matrix. Instead of using any block permutation matrix as in [1], we propose to solve the SE (7) row-by-row (i.e., band-by-band). Recall the following lemma introduced in [1].

Lemma 1 (*Wei et al. [1]):* The following equality holds

$$\mathbf{F}^H \underline{\mathbf{S}} \mathbf{F} = \frac{1}{d} \mathbf{J}_d \otimes \mathbf{I}_m \tag{8}$$

where $\mathbf{F}$ and $\underline{\mathbf{S}}$ are defined as in Section III-A, $\mathbf{J}_d$ is the $d \times d$ matrix of ones and $\mathbf{I}_m$ is the $m \times m$ identity matrix.

By simply decomposing matrix $\mathbf{J}_d$ as $\mathbf{J}_d = \mathbf{1}_d \mathbf{1}_d^T$, where $\mathbf{1}_d \in \mathbb{R}^d$ is a vector of ones and using the mixed-product property of Kronecker product, i.e., $(\mathbf{A}_1\mathbf{A}_2) \otimes (\mathbf{A}_3\mathbf{A}_4) = (\mathbf{A}_1 \otimes \mathbf{A}_3)(\mathbf{A}_2 \otimes \mathbf{A}_4)$ (if $\mathbf{A}_1$, $\mathbf{A}_2$, $\mathbf{A}_3$ and $\mathbf{A}_4$ are matrices of proper sizes), we can easily obtain the following result

$$\mathbf{F}^H \underline{\mathbf{S}} \mathbf{F} = \frac{1}{d} (\mathbf{1}_d \otimes \mathbf{I}_m)(\mathbf{1}_d^T \otimes \mathbf{I}_m). \tag{9}$$

Substituting (9) into (7) leads to

$$\mathbf{\Lambda}\bar{\mathbf{U}} + \bar{\mathbf{U}}\mathbf{M} = \bar{\mathbf{C}} \tag{10}$$

where $\bar{\mathbf{U}} = \mathbf{Q}^{-1}\mathbf{UF}, \mathbf{M} = \frac{1}{d}\bar{\mathbf{D}}\bar{\mathbf{D}}^H, \bar{\mathbf{D}} = \mathbf{D}(\mathbf{1}_d \otimes \mathbf{I}_m)$, and $\bar{\mathbf{C}} = \mathbf{Q}^{-1}\mathbf{CF}$. Equation (10) is an SE w.r.t. $\bar{\mathbf{U}}$ whose solution is significantly easier than the one of (6), due to the simple structure of matrix $\mathbf{M}$. To ease the notation, the diagonal matrices $\mathbf{\Lambda}$ and $\mathbf{D}$ are rewritten as $\mathbf{\Lambda} = \text{diag}(\lambda_1, \ldots, \lambda_{\widetilde{m}_\lambda})$ and $\mathbf{D} = \text{diag}(\mathbf{D}_1, \ldots, \mathbf{D}_d)$, where $\text{diag}(\cdot_1, \ldots, \cdot_k)$ represents a (block) diagonal matrix whose diagonal blocks are $\cdot_1, \ldots, \cdot_k$ and $\lambda_i \geq 0 \forall i$. Thus, we have $\bar{\mathbf{D}}^H\bar{\mathbf{D}} = \sum_{t=1}^d \mathbf{D}_t^H\mathbf{D}_t = \sum_{t=1}^d \mathbf{D}_t^2$.

In the following, we will show that (10) can be solved row-by-row explicitly. First, we rewrite $\bar{\mathbf{U}}$ and $\bar{\mathbf{C}}$ as $\bar{\mathbf{U}} = [\bar{\mathbf{u}}_1^T, \ldots, \bar{\mathbf{u}}_{\widetilde{m}_\lambda}^T]^T$ and $\bar{\mathbf{C}} = [\bar{\mathbf{c}}_1^T, \ldots, \bar{\mathbf{c}}_{\widetilde{m}_\lambda}^T]^T$, where $\bar{\mathbf{u}}_i \in \mathbb{R}^{1\times n}$ and $\bar{\mathbf{c}}_i \in \mathbb{R}^{1\times n}$ are row vectors. Using these notations, (10) can be decomposed as

$$\lambda_i \bar{\mathbf{u}}_i + \bar{\mathbf{u}}_i \mathbf{M} = \bar{\mathbf{c}}_i$$

for $i = 1, \ldots, \widetilde{m}_\lambda$. Straightforward computations lead to

$$\bar{\mathbf{u}}_i = \bar{\mathbf{c}}_i (\mathbf{M} + \lambda_i \mathbf{I}_n)^{-1}. \tag{11}$$

Following the Woodbury formula [23] and using $\bar{\mathbf{D}}^H\bar{\mathbf{D}} = \sum_{t=1}^d \mathbf{D}_t^2$, the inversion in (11) can be easily computed as $(\mathbf{M} + \lambda_i \mathbf{I}_n)^{-1} = \lambda_i^{-1}\mathbf{I}_n - \lambda_i^{-1}\bar{\mathbf{D}}(\lambda_i d\mathbf{I}_m + \sum_{t=1}^d \mathbf{D}_t^2)^{-1}\bar{\mathbf{D}}^H$. As $\lambda_i d\mathbf{I}_m + \sum_{i=1}^d \mathbf{D}_i^2$ is a real diagonal matrix, its inverse is easy to be computed with a complexity of order $\mathcal{O}(m)$. Using this simple inversion, the solution $\bar{\mathbf{U}}$ of the SE (10) can be computed row-by-row (band-by-band) as

$$\bar{\mathbf{u}}_i = \lambda_i^{-1}\bar{\mathbf{c}}_i - \lambda_i^{-1}\bar{\mathbf{c}}_i\bar{\mathbf{D}}\left(\lambda_i d\mathbf{I}_m + \sum_{t=1}^d \mathbf{D}_t^2\right)^{-1}\bar{\mathbf{D}}^H \tag{12}$$

for $i = 1, \ldots, \widetilde{m}_\lambda$. The final estimator of $\mathbf{X}$ is obtained as

$$\hat{\mathbf{X}} = \mathbf{HQ}\bar{\mathbf{U}}\mathbf{F}^H.$$

C. Difference with [1]

It is interesting to mention some important differences between the proposed R-FUSE strategy and the one of [1]

1) The matrix $\mathbf{B}$ (or $\mathbf{D}$) is not required to be invertible.
2) Each band can be restored as a whole instead of block by block (d blocks).

Algorithm 1: Robust Fast fUsion based on solving a Sylvester Equation (R-FUSE)

Input: $\mathbf{Y}_\text{L}$, $\mathbf{Y}_\text{R}$, $\mathbf{\Lambda}_\text{L}$, $\mathbf{\Lambda}_\text{R}$, $\mathbf{L}$, $\mathbf{B}$, $\mathbf{S}$, $\mathbf{H}$, d

$\mathbf{D} \leftarrow \text{EigDec}(\mathbf{B})$; // *FFT transformation*

$\bar{\mathbf{D}} \leftarrow \mathbf{D}(\mathbf{1}_d \otimes \mathbf{I}_m)$;

$\mathbf{C}_1 \leftarrow \mathbf{C}_1(\mathbf{H}, \mathbf{L}, \mathbf{\Lambda}_\text{L}, \mathbf{\Lambda}_\text{R})$; // *Compute cf.* (5)

$(\mathbf{Q}, \mathbf{\Lambda}) \leftarrow \text{EigDec}(\mathbf{C}_1)$; // *cf.* $\mathbf{C}_1 = \mathbf{Q\Lambda Q}^{-1}$

$\mathbf{C} \leftarrow \mathbf{C}(\mathbf{H}, \mathbf{L}, \mathbf{\Lambda}_\text{L}, \mathbf{\Lambda}_\text{R}, \mathbf{Y}_\text{L}, \mathbf{Y}_\text{R}, \mathbf{B}, \mathbf{S})$; // *cf.* (5)

$\bar{\mathbf{C}} \leftarrow \mathbf{Q}^{-1}\mathbf{CF}$;

// *Compute* $\bar{\mathbf{U}}$ *band by band* ($\widetilde{m}_\lambda$ *bands)*

for $l = 1$ **to** $\widetilde{m}_\lambda$ **do**

  $\bar{\mathbf{u}}_i \leftarrow \bar{\mathbf{u}}_i(\lambda_i, d, \bar{\mathbf{c}}_i, \bar{\mathbf{D}}, \mathbf{D})$; // *cf.* (12)

end

Set $\hat{\mathbf{X}} = \mathbf{HQ}\bar{\mathbf{U}}\mathbf{F}^H$;

Output: $\hat{\mathbf{X}}$

Algorithm 1 summarizes the derived R-FUSE steps required to calculate the estimated image $\hat{\mathbf{X}}$, where the different parts compared with [1] have been highlighted in red.

D. Complexity Analysis

The most computationally expensive part of the proposed algorithm is the computation of the matrix $\bar{\mathbf{C}}$ (because of the FFT and iFFT operations), which has a complexity of order $\mathcal{O}(\widetilde{m}_\lambda n \log n)$. The left matrix multiplications with $\mathbf{Q}^{-1}$ (to compute $\bar{\mathbf{C}}$) and with $\left(\mathbf{H}^H\mathbf{\Lambda}_\text{R}^{-1}\mathbf{H}\right)^{-1}$ (to compute $\mathbf{C}$) have a complexity of order $\mathcal{O}(\widetilde{m}_\lambda^2 n)$. Thus, the calculation of $\bar{\mathbf{C}}$ has a total complexity of order $\mathcal{O}(\widetilde{m}_\lambda n \cdot \max\{\log n, \widetilde{m}_\lambda\})$, which can be approximated by $\mathcal{O}(\widetilde{m}_\lambda n \log n)$ as $\log n \gg \widetilde{m}_\lambda$.

Note that the proposed R-FUSE scheme can be embedded within an ADMM or a BCD algorithm to deal with Bayesian estimators, as explained in [1].

IV. Experimental Results

This section applies the proposed fusion method to two Bayesian fusion schemes (with appropriate priors for the unknown matrix $\mathbf{X}$) that have been investigated in [11] and [12]. Note that these two methods require to solve a minimization problem similar to (2). All the algorithms have been implemented using MATLAB R2015b on a computer with Intel(R) Core i7-4790 CPU@3.60 GHz and 16 GB RAM.

A. Fusion Quality Metrics

Following [10] and [13], we used the restored signal-to-noise ratio (RSNR), the averaged spectral angle mapper (SAM), the universal image quality index (UIQI), the relative dimensionless global error in synthesis (ERGAS), and the degree of distortion (DD) as quantitative measures to evaluate the quality of the fused results. The larger RSNR and UIQI, or the smaller SAM, ERGAS, and DD, the better the fusion.

B. Fusion of Multiband Images

The reference image considered here as the high-spatial and high-spectral image is a $512 \times 256 \times 93$ HS image acquired

Fig. 1. Pavia dataset: (left) HS image, (middle) MS image, and (right) reference image.

Fig. 2. HS+MS fusion results. From left to right: (1st) FUSE using Gaussian prior, (2nd) R-FUSE using Gaussian, (3rd) FUSE using TV, and (4th) R-FUSE using TV.

TABLE I
PERFORMANCE OF HS+MS FUSION METHODS: RSNR (IN DB), UIQI, SAM (IN DEGREE), ERGAS, DD (IN 10^{-3}), AND TIME (IN SECOND)

Prior	Methods	RSNR	UIQI	SAM	ERGAS	DD	Time
Gaussian	FUSE	29.243	0.9904	1.513	0.902	6.992	0.27
	R-FUSE	29.243	0.9904	1.513	0.902	6.992	0.24
TV	FUSE	29.629	0.9914	1.456	0.853	6.761	133
	R-FUSE	29.629	0.9914	1.456	0.853	6.761	115

over Pavia, Italy, by the reflective optics system imaging spectrometer (ROSIS). This image was initially composed of 115 bands that have been reduced to 93 bands after removing the water vapor absorption bands. A composite color image of the scene of interest is shown in Fig. 1(right).

First, $\mathbf{Y}_{\mathrm{R}}$ has been generated by applying a 5×5 Gaussian filter [see Fig. 3(left)] and by down-sampling every 4 pixels in both vertical and horizontal directions for each band of the reference image. Second, a 4-band MS image $\mathbf{Y}_{\mathrm{L}}$ has been obtained by filtering $\mathbf{X}$ with the LANDSAT-like reflectance spectral responses [24]. The HS and MS images are both contaminated by zero-mean additive i.i.d. Gaussian noises with $\mathrm{SNR}_{\mathrm{H}} = 40$ dB for HS bands and $\mathrm{SNR}_{\mathrm{M}} = 30$ dB for MS bands. The observed HS and MS images are shown in Fig. 1(left and middle).

We consider the Bayesian fusion with Gaussian [10] and total variation (TV) [12] priors that were considered in [1]. The subspace matrix $\mathbf{H}$ was estimated using PCA as in [1]. The proposed R-FUSE and FUSE algorithms are compared in terms of their performance and computational time for the same optimization problem (corresponding to (18) in [1]). The estimated images obtained with the different algorithms are depicted in Fig. 2 and are visually very similar. The corresponding quantitative results are reported in Table I, which confirms the same performance of FUSE and R-FUSE in terms of the various fusion quality measures (see [10] for the definitions of RSNR, UIQI, SAM, ERGAS, and DD). Note that the results associated with a TV prior are slightly better than the ones obtained with a Gaussian prior, which can be attributed to the well-known discontinuity preserving ability of the TV prior. A particularity of the R-FUSE algorithm is its reduced computational complexity due to the avoidance of any permutation in the frequency domain when solving the Sylvester matrix equation, as demonstrated by the computational time also reported in Table I. More simulation results on different datasets can be found in the technical report [25].

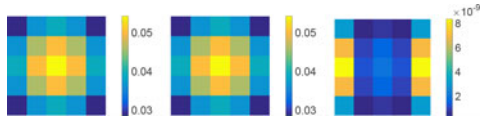

Fig. 3. (Left) Blurring kernel used in Section IV-B, (middle) blurring kernel used in Section IV-C, and (right) their difference.

TABLE II
PERFORMANCE OF HS+MS FUSION METHODS WITH A SLIGHTLY DIFFERENT KERNEL: RSNR (IN DB), UIQI, SAM (IN DEGREE), ERGAS, DD (IN 10^{-3}), AND TIME (IN SECOND)

Prior	Methods	RSNR	UIQI	SAM	ERGAS	DD	Time
TV	FUSE	9.985	0.5640	14.50	8.348	74.7	133
	R-FUSE	29.629	0.9914	1.456	0.853	6.761	115

C. Robustness w.r.t. the Blurring Kernel

In this section, we consider a kernel similar to the one used in Section IV-B, which is displayed in Fig. 3(middle) (the difference between the two kernels is shown in the right). Note that this trivial change is such that the FT of the new kernel has some values that are very close to zero. Due to the inversion of $\mathbf{B}$ in FUSE, this slight change can dramatically impact the performance of the FUSE algorithm. The fusion performance of FUSE and R-FUSE with a TV prior is summarized in Table II. Obviously, the performance of FUSE degrades a lot due to the presence of close-to-zero values in the kernel FT, which does not agree with the invertibility assumption of $\mathbf{B}$. On the contrary, the proposed R-FUSE provides results very close to (almost the same with) those obtained in Section IV-B, demonstrating its robustness w.r.t. the blurring kernel.

V. CONCLUSION

This letter developed a new robust and faster multiband image fusion method based on the resolution of a generalized SE. The application of the Woodbury formula allows any permutation in the frequency domain to be avoided and brings two benefits. First, the invertibility assumption of the blurring operator is not necessary, leading to a more robust fusion strategy. Second, the computational complexity of the fusion algorithm is reduced. Similar to the method in [1], the proposed algorithm can be embedded into a BCD or an ADMM to implement (hierarchical) Bayesian fusion models. Numerical experiments confirmed that the proposed robust fast fusion method has the advantage of reducing the computational cost and also is more robust to the blurring kernel conditioning, compared with the method investigated in [1].

REFERENCES

[1] Q. Wei, N. Dobigeon, and J.-Y. Tourneret, "Fast fusion of multi-band images based on solving a Sylvester equation," *IEEE Trans. Image Process.*, vol. 24, no. 11, pp. 4109–4121, Nov. 2015.

[2] L. Loncan *et al*., "Hyperspectral pansharpening: A review," *IEEE Geosci. Remote Sens. Mag.*, vol. 3, no. 3, pp. 27–46, Sep. 2015.

[3] C.-I. Chang, *Hyperspectral Data Exploitation: Theory and Applications*. New York, NY, USA: Wiley, 2007.

[4] H. Aanaes, J. Sveinsson, A. Nielsen, T. Bovith, and J. Benediktsson, "Model-based satellite image fusion," *IEEE Trans. Geosci. Remote Sens.*, vol. 46, no. 5, pp. 1336–1346, May 2008.

[5] T. Stathaki, *Image Fusion: Algorithms and Applications*. New York, NY, USA: Academic, 2011.

[6] M. Gong, Z. Zhou, and J. Ma, "Change detection in synthetic aperture radar images based on image fusion and fuzzy clustering," *IEEE Trans. Image Process.*, vol. 21, no. 4, pp. 2141–2151, Apr. 2012.

[7] A. P. James and B. V. Dasarathy, "Medical image fusion: A survey of the state of the art," *Inf. Fusion*, vol. 19, pp. 4–19, 2014.

[8] B. Aiazzi, L. Alparone, S. Baronti, A. Garzelli, and M. Selva, "25 years of pansharpening: A critical review and new developments," in *Signal and Image Processing for Remote Sensing*, 2nd ed., C. H. Chen, Ed. Boca Raton, FL, USA: CRC Press, 2011, ch. 28, pp. 533–548.

[9] A. Gupta and D. Nagar, *Matrix Variate Distributions (Monographs and Surveys in Pure and Applied Mathematics)*. Taylor & Francis, 1999.

[10] Q. Wei, N. Dobigeon, and J.-Y. Tourneret, "Bayesian fusion of multi-band images," *IEEE J. Sel. Topics Signal Process.*, vol. 9, no. 6, pp. 1117–1127, Sep. 2015.

[11] Q. Wei, N. Dobigeon, and J.-Y. Tourneret, "Bayesian fusion of multispectral and hyperspectral images using a block coordinate descent method," in *Proc. IEEE GRSS Workshop Hyperspectral Image Signal Process.: Evol. Remote Sens.*, Tokyo, Japan, pp. 1714–1719, Jun. 2015.

[12] M. Simoes, J. Bioucas-Dias, L. Almeida, and J. Chanussot, "A convex formulation for hyperspectral image superresolution via subspace-based regularization," *IEEE Trans. Geosci. Remote Sens.*, vol. 53, no. 6, pp. 3373–3388, Jun. 2015.

[13] Q. Wei, J. Bioucas-Dias, N. Dobigeon, and J.-Y. Tourneret, "Hyperspectral and multispectral image fusion based on a sparse representation," *IEEE Trans. Geosci. Remote Sens.*, vol. 53, no. 7, pp. 3658–3668, Jul. 2015.

[14] M. Afonso, J. M. Bioucas-Dias, and M. Figueiredo, "An augmented Lagrangian approach to the constrained optimization formulation of imaging inverse problems." *IEEE Trans. Image Process.*, vol. 20, no. 3, pp. 681–95, Mar. 2011.

[15] Q. Wei, N. Dobigeon, and J.-Y. Tourneret, "Fast fusion of multi-band images based on solving a Sylvester equation—Complementary results and supporting materials," Univ. of Toulouse, Toulouse, France, *IRIT/INP-ENSEEIHT, Tech. Rep.*, Jun. 2015. [Online]. Available: http://wei.perso.enseeiht.fr/papers/2015-WEI-TR-Sylvester.pdf

[16] N. Zhao, Q. Wei, A. Basarab, N. Dobigeon, D. Kouamé, and J.-Y. Tourneret, "Fast single image super-resolution using a new analytical solution for $\ell_2 - \ell_2$ problems," *IEEE Trans. Image Process.*, vol. 25, no. 8, pp. 3683–3697, Aug. 2016.

[17] N. Zhao, Q. Wei, A. Basarab, D. Kouamé, and J.-Y. Tourneret, "Single image super-resolution of medical ultrasound images using a fast algorithm," in *Proc. IEEE Int. Symp. Biomed. Imaging*, Apr. 2016, pp. 473–476.

[18] C.-I. Chang, X.-L. Zhao, M. L. Althouse, and J. J. Pan, "Least squares subspace projection approach to mixed pixel classification for hyperspectral images," *IEEE Trans. Geosci. Remote Sens.*, vol. 36, no. 3, pp. 898–912, May 1998.

[19] J. M. Bioucas-Dias and J. M. Nascimento, "Hyperspectral subspace identification," *IEEE Trans. Geosci. Remote Sens.*, vol. 46, no. 8, pp. 2435–2445, Aug. 2008.

[20] R. Neelamani, H. Choi, and R. Baraniuk, "ForWaRD: Fourier-wavelet regularized deconvolution for ill-conditioned systems," *IEEE Trans. Signal Process.*, vol. 52, no. 2, pp. 418–433, Feb. 2004.

[21] Y. Wang, J. Yang, W. Yin, and Y. Zhang, "A new alternating minimization algorithm for total variation image reconstruction," *SIAM J. Imaging Sci.*, vol. 1, no. 3, pp. 248–272, 2008.

[22] R. H. Bartels and G. Stewart, "Solution of the matrix equation AX+ XB= C," *Commun. ACM*, vol. 15, no. 9, pp. 820–826, 1972.

[23] M. A. Woodbury, "Inverting modified matrices, ",*Memorandum Rep.*, vol. 42. Princeton, NJ, USA: Princeton Univ. Press, p. 106, 1950.

[24] D. Fleming, "Effect of relative spectral response on multi-spectral measurements and NDVI from different remote sensing systems," *Ph.D. dissertation*, Dept. Geography, Univ. Maryland, College Park, MD, USA, 2006.

[25] Q. Wei, N. Dobigeon, J.-Y. Tourneret, J. Bioucas-Dias, and S. Godsill, "R-fuse: Robust fast fusion of multi-band images based on solving a Sylvester equation—Complementary results and supporting materials," Dept. Eng., Univ. Cambridge, Cambridge, U.K., *Tech. Rep.*, Jul. 2016. [Online]. Available: http://sigproc.eng.cam.ac.uk/foswiki/pub/Main/QW245/WEI_SPL_TR_20160714.pdf.